Physics of forced magnetic reconnection in coaxial helicity injection experiments in National Spherical Torus Experimenta)

F. Ebrahimi, R. Raman, E. B. Hooper, C. R. Sovinec, and A. Bhattacharjee

Citation: Physics of Plasmas (1994-present) **21**, 056109 (2014); doi: 10.1063/1.4875337
View online: http://dx.doi.org/10.1063/1.4875337
View Table of Contents: http://scitation.aip.org/content/aip/journal/pop/21/5?ver=pdfcov
Published by the AIP Publishing

Physics of forced magnetic reconnection in coaxial helicity injection experiments in National Spherical Torus Experiment[a)]

F. Ebrahimi,[1,b)] R. Raman,[2] E. B. Hooper,[3] C. R. Sovinec,[4] and A. Bhattacharjee[1]
[1]*Department of Astrophysical Sciences, and Princeton Plasma Physics Laboratory, Princeton University, New Jersey 08544, USA*
[2]*University of Washington, Seattle, Washington 98195, USA*
[3]*Lawrence Livermore National Laboratory, Livermore, California 94526, USA*
[4]*University of Wisconsin, Madison, Wisconsin 53706, USA*

(Received 15 January 2014; accepted 21 March 2014; published online 6 May 2014)

We numerically examine the physics of fast flux closure in transient coaxial helicity injection (CHI) experiments in National Spherical Torus Experiment (NSTX). By performing resistive Magnetohydrodynamics (MHD) simulations with poloidal injector coil currents held constant in time, we find that closed flux surfaces are formed through forced magnetic reconnection. Through a local Sweet-Parker type reconnection with an elongated current sheet in the injector region, closed flux surfaces expand in the NSTX global domain. Simulations demonstrate outflows approaching poloidally Alfvénic flows and reconnection times consistent with the Sweet-Parker model. Critical requirements for magnetic reconnection and flux closure are studied in detail. These primary effects, which are magnetic diffusivity, injector flux, injector flux footprint width, and rate of injector voltage reduction, are simulated for transient CHI experiments. The relevant time scales for effective reconnection are $\tau_V < \tau_{rec} \approx \tau_A \sqrt{S}(1+Pm)^{1/4} < \tau_R$, where τ_V is the time for the injector voltage reduction, τ_A is the poloidal Alfvén transit time, τ_R is the global resistive diffusion time, and Pm and S are Prandtl and Lundquist numbers. © *2014 AIP Publishing LLC*. [http://dx.doi.org/10.1063/1.4875337]

I. INTRODUCTION

Conventional tokamak designs rely on a central solenoid to generate an inductive initial current. However, due to the restricted space for a central solenoid in a low aspect ratio Spherical Torus (ST), elimination of the central solenoid is likely necessary for an ST based reactor or a component test facility.[1–4] Solenoid free non-inductive current start-up techniques could also simplify a reactor based on the tokamak concept and various radio-frequency schemes have been investigated.[5–7] Coaxial Helicity Injection (CHI) is a leading candidate for plasma start-up and current formation in NSTX. Understanding the dynamics and the mechanism of closed flux surface formation during transient CHI is of great importance and has been an outstanding problem for a long time. In a systematic approach undertaken recently, the fundamental reconnection mechanism that leads to the generation of closed flux surfaces in a transient CHI discharge was explained.[8] It was shown that the reconnection process and closed flux surfaces during transient CHI can be explained through 2-D Sweet-Parker type reconnection.[9,10] Here, using resistive MHD simulations in a more comprehensive study, we examine the physics of fast flux closure in transient CHI experiments in NSTX. Through global simulations in the domain of the experiment, we investigate both local and global characteristics of magnetic reconnection during transient CHI, including reconnection time and outflows. We also find the critical MHD requirements for fast flux closure.

CHI as a form of electrostatic helicity injection has been the most tested solenoid-free plasma start-up method in NSTX. In electrostatic helicity injection, helicity is injected by driving current along open field lines that connect two electrodes. Figure 1 describes the implementation of CHI on NSTX. The initial poloidal field, the injector flux, connecting the inner and outer divertor plates in the injector region is produced using the lower divertor coils, as shown in Fig. 1. The inner and outer divertor plates are electrically separated by two toroidal insulators located at the top and bottom of the machine. In the presence of a toroidal magnetic field, gas is injected in the lower part of the divertor plates (injector region), and a biased voltage (V_{inj}) is applied to the inner and outer divertor plates. By driving current along the open field lines (the injector current I_{inj}), helicity is injected through the linkage of toroidal flux that links the poloidal injector flux. Because in an ST, the toroidal flux that links the injector flux is composed of both the injector current produced toroidal flux, and the toroidal flux generated by the toroidal field coil, both these are injected. It can be shown that the helicity injection rate is twice the product of the biased injector voltage and flux, $\dot{K} = 2\Psi_{inj}V_{inj}$.[11] Plasma and open field lines (the magnetic bubble) expand into the vessel if the injector current exceeds a threshold value. This occurs when the Lorentz force $J_{pol} \times B_{tor}$ exceeds the field line tension of the injector flux.[12,13] In transient CHI, right after the magnetic bubble fills up the vessel (reaches the top of the vessel referred to as the absorber region), the injector voltage is rapidly reduced to zero. At this time, the field lines in the injector region reconnect and a high quality closed flux start-up equilibrium is generated in NSTX.[14,15] This process happens fast, in about 2.5 ms. This new method of *transient* CHI in an ST was first demonstrated on the HIT-II experiment at the

[a)]Paper PI2 2, Bull. Am. Phys. Soc. **58**, 234 (2013).
[b)]Invited speaker.

University of Washington, and later successfully tested and further developed on the NSTX device at PPPL. In contrast, in the conventional CHI approach, some of the injector current is maintained and used to drive current along the open field lines. One then relies on non-axisymmetric MHD activity to drive current on closed field lines through the action of a dynamo current drive mechanism. This approach, known as *driven* CHI, is being currently investigated in small machines,[16,17] and also being studied through MHD simulations.[18]

This paper is organized as follows. The computational model is described in Sec. II. The simulation results for the effects of magnetic diffusivity, injector flux, injector flux footprint width, and the rate of injection voltage reduction on flux closure are presented and discussed in Secs. III–VI, respectively. Simulations with temperature evolution are presented in Sec. VII. We then summarize the main results in Sec. VIII.

II. THE COMPUTATIONAL MODEL

To study helicity injection, we perform axisymmetric time-dependent resistive MHD simulations using the NIMROD code.[20] In this paper, we use the same helicity injection model, boundary condition and geometry as in our earlier papers.[8,19] Axisymmetric ($n=0$) simulations with poloidal grid 45×90 fourth or fifth order finite elements are performed in the geometry of the experiment with a narrow slot of 4 cm (Fig. 2). The temporal resolution is automatically adjusted to keep the flow-CFL condition below a specified bound. Time steps vary from approximately a microsecond down to as small as a nanosecond. Throughout this paper, the initial injector flux is generated by including NSTX poloidal coil currents, which are kept fixed in time (with fixed boundary field). In all our simulations (except the simulations in Sec. VI), a uniform voltage is applied across the injector gap at $t=6$ ms and turned off at 9 ms. The

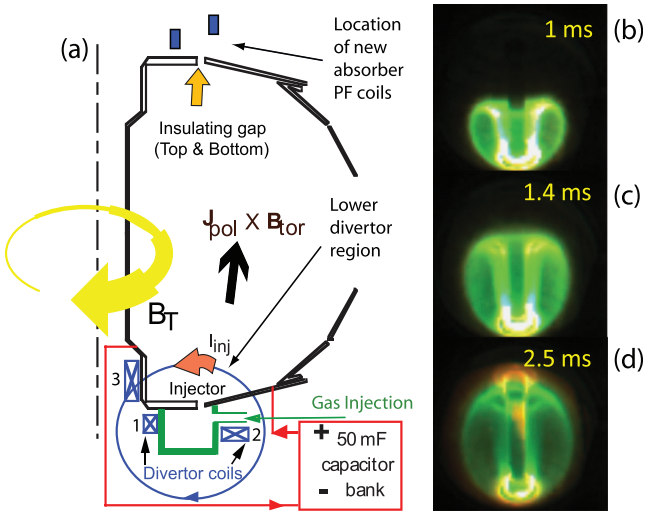

FIG. 1. (a) To the left is a line drawing showing the main components in NSTX required for plasma start-up using the CHI method. Top-right (b) fast camera fish-eye image of the plasma during the early phase of plasma growth, (c) as the discharge grows, and (d) after it fills the vessel. The times are referenced to the capacitor bank discharge time. The numbers 1, 2, and 3 in the figure near the words divertor coils indicate the coils used to setup the initial injector flux configuration. They are: (1) the PF1B injector coil, (2) the PF2L flux-shaping coil, and (3) the PF1AL flux-shaping coil.

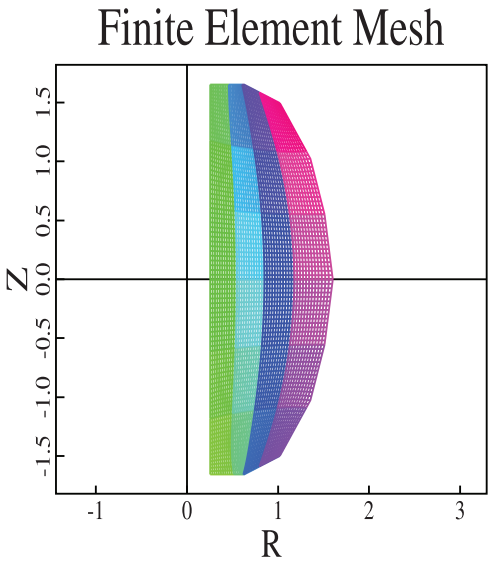

FIG. 2. Computational finite-element grid used in the simulations. Grid packing used around the injector gap (R = 0.59 m–0.63 m). See Ref. 19 for more details.

absorber voltage in the simulations is determined by requiring the total toroidal flux to be constant in time inside the vessel.[19] The normal flows at the injector and absorber gap are E × B flows. We perform zero pressure simulations where temperature and number density are not evolved. To facilitate comparison with experimental conditions for each simulation at uniform magnetic diffusivity (resistivity), constant temperature values are specified. A uniform number density of $4 \times 10^{18}\,\mathrm{m}^{-3}$ for a deuterium plasma is used. Simulations where plasma temperature is evolved are presented in Sec. VIII. Simulations in this paper are axisymmetric ($n=0$). We have performed simulations including non-axisymmetric $n=1$ mode in both zero pressure and finite pressure cases, and no significant effect was found.

III. MAGNETIC DIFFUSIVITY AND PHYSICS OF MAGNETIC RECONNECTION

In an earlier study, the magnetic reconnection process and the mechanism for generation of closed flux surfaces during transient CHI was described.[8] It was found that at sufficiently low magnetic diffusivity (high Lundquist number), the oppositely directed field lines in the injector region have sufficient time to reconnect (before dissipating), leading to the formation of closed flux surfaces. Simulations at magnetic diffusivities (temperatures) similar to those in the experiment showed X point formation, followed by formation of closed flux surfaces after the driven injector voltage is turned off. The key physics that triggers magnetic reconnection was also explained. It was found that, as the injector voltage is turned off, the field lines tend to untwist in the toroidal direction and magnetic field compression exerts a radial $J \times B$ force to bring oppositely directed field lines closer together to reconnect.[8,19]

The reconnection process was shown to have transient Sweet-Parker characteristics.[8] Two key signatures of Sweet-Parker reconnection, an elongated current sheet and an $\eta^{1/2}$ scaling was demonstrated through the characteristics of

simulations results. It was shown that during X point formation, an elongated current sheet is formed and its width scales with magnetic diffusivity close to $\eta^{1/2}$, consistent with Sweet-Parker reconnection. Here, we further investigate the nature of the reconnection through the characteristics of the outflows and reconnection time scales obtained in the simulations.

In the resistive MHD model of magnetic reconnection, magnetic diffusivity (resistivity) becomes important around the magnetic field null and causes the fields lines to reconnect. Here, we find that magnetic diffusivity also has a critical effect in the reconnection process in transient CHI. However, due to the transient nature of this process, for formation of closed flux surfaces, substantial reconnection should occur before the established open field line configuration dissipates because the open-field lines current is rapidly decreasing in time. This means that the resistive diffusion time for the global currents should be much longer than the reconnection time. Figure 3 shows the ratio of closed current (current in the closed flux region) to the total plasma current obtained from several simulations by varying the injector current and magnetic diffusivity. It shows that the ratio of the closed current to the total plasma current, which is similar to that of the ratio of the closed poloidal flux to the total poloidal flux. Using the Spitzer resistivity relation with temperature, $\eta[\mathrm{m}^2/\mathrm{s}] = 410 T_e^{-3/2}[\mathrm{eV}]$ (using Coulomb logarithm of $\lambda = 10$), we have used the equivalent temperature values for the magnetic diffusivities. In these simulations, to obtain a fixed injector current for a specific amount of injector flux, a higher injector voltage (V_{inj}) is required as the magnetic diffusivity is increased. This is because the resistance of the field lines now increases and so a higher voltage is necessary to attain the same value of injector current. For injecting poloidal magnetic flux (and helicity) into the vessel, it is necessary to satisfy the "bubble burst" condition. This condition[12] states that for a given combination of injector flux and toroidal field, a minimum level of injector current, known as the bubble burst current, is required. Experimentally, the applied voltage is adjusted to achieve this current. Thus, for example, on the same machine if increased impurities on the electrode surfaces increase the plasma resistivity, then a higher voltage needs to be applied to satisfy the bubble burst criterion. This is consistent with the simulation results in Fig. 3. First for a given plasma resistivity, a minimum injector current (controlled by the injector voltage) is required for the magnetic flux to fill up the vessel. Second, for reconnection to occur, the injector current should be even higher, depending on the value of plasma resistivity (or temperature).

We find that, for a given amount of injected helicity, there is a critical temperature below which closed flux surfaces do not form (Fig. 4). At temperatures below a critical value, for example for the case in Fig. 3, the global resistive diffusion time ($\tau_R = a^2/\eta \approx 3.6\,\mathrm{ms}$ with $\mathrm{a} = 0.6\,\mathrm{m}$ and $\eta = 100\,\mathrm{m}^2/\mathrm{s}$) is too fast, which causes any reconnected flux to decay away must faster than the closed flux surfaces form, so that little or no closed flux surfaces are seen in the

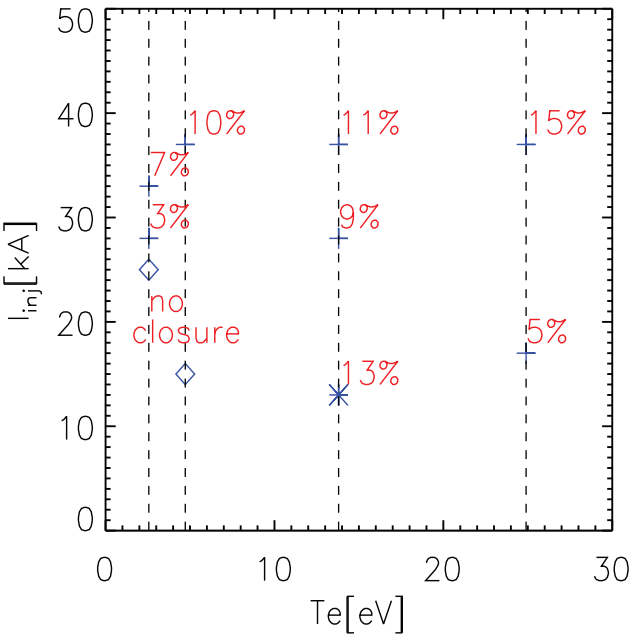

FIG. 3. Injector current (I_{inj}) and closed flux fraction as a function of Te. The ratio of closed current to the total current for several simulations is shown by the numbers in the figure. Crosses show simulations with $\Psi_{\mathrm{inj}} \sim 55\,\mathrm{mWb}$ with reconnection, diamonds show no flux closure. Asterisk is for simulation with $\Psi_{\mathrm{inj}} \sim 22\,\mathrm{mWb}$ with narrow footprint (presented in Sec. V) Pm = 7.5. These simulations also show that for a given value of the injector flux, there is a threshold for the injector current, below which only some of the injector flux (and helicity) is injected into the vessel, which also results in less closed flux current being generated. This can be seen from the simulations at $Te \sim 2.5 - 5\,\mathrm{eV}$, where the magnitude of closed flux current increases with the injector current, and there is no flux closure below I_{inj} of about 25 kA.

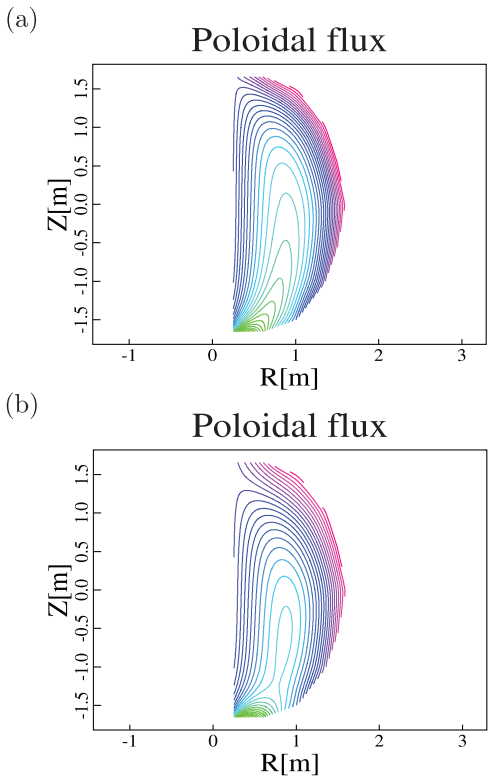

FIG. 4. Flux surfaces for $\eta = 100\mathrm{m}^2/\mathrm{s}\,(T_e \approx 2.7\,\mathrm{eV})$ with $I_{\mathrm{inj}} = 28\,kA$ and $\Psi_{\mathrm{inj}} \sim 55\,\mathrm{mWb}$ (a) at $\mathrm{t} = 9\,\mathrm{ms}$, injector flux has filled up the vessel, and (b) at $\mathrm{t} = 9.19\,\mathrm{ms}$. The small amount of reconnected flux decays very fast after $\mathrm{t} = 9.19\,\mathrm{ms}$.

simulations (Fig. 3(b)). Finally, it is also found that when reconnection occurs, the ratio of closed current to plasma current increases with temperature (Fig. 3). For example at $I_{inj} \approx 28$kA, this ratio increases from 3% to 9% when temperature is increased from 2.7 eV to 14 eV, or at $I_{inj} \approx 37$kA, where the ratio of closed current is largest ($\approx$15%) for higher temperature ($\approx$24 eV) as shown in Fig. 3. At the higher value of injector current, more helicity (and poloidal flux) is injected. This in combination with the higher temperature results in a higher fraction of closed flux current. Typical flux surfaces at higher temperature with formation of fairly large volume of flux surfaces are shown in Fig. 5.

Magnetic diffusivity also enters the reconnection time. First, for our problem, the Sweet-Parker reconnection time in a visco-resistive plasma can be obtained from $t_{rec} \sim a/V_{in}$, when the following four conditions are combined (note that a is an arbitrary macroscopic length); (1) the conservation of the mass $V_{out}\delta \sim V_{in}L$, where δ and L are the width and length of the elongated current sheet shown in Fig. 6(a), (2) by matching the electric fields outside and inside the reconnection layer, $V_{in}B_{in} \sim \eta\mu_0 J$, to give $V_{in} \sim \eta/\delta$, (3) force balance equation $[\rho \mathbf{V}.\nabla\mathbf{V} = -\nabla(B_R^2 + B_z^2 + B_\phi^2)/2\mu_0 + (\mathbf{B}\cdot\nabla\mathbf{B})/\mu_0 + \rho\nu\nabla^2\mathbf{V}]$ in the direction of current sheet (Z), $\rho V_{out}^2/L \sim B_{in}B_{out}/\mu_0\delta - \nu\rho V_{out}/\delta^2$, (4) from $\nabla\cdot B = 0$, to give $B_{out}/\delta \sim B_{in}/L$. Here, V_{in} and V_{out} are flows in the (R) and (Z) directions, respectively, and B_{in} and B_{out} are magnetic fields in the (Z) and (R) directions, respectively. From these four conditions, we then obtain the Sweet-Parker outflow $V_{out}/V_{A(in)} = 1/\sqrt{1+Pm}$ and the reconnection time $t_{rec} \sim \sqrt{\tau_A\tau_R}(1+Pm)^{1/4} = \tau_A\sqrt{S}(1+Pm)^{1/4}$, where $V_{A(in)} = B_{in}/\sqrt{\mu_0\rho}$, $Pm = \nu/\eta$, and $S = \tau_R V_A/a$ are the Alfvén velocity, magnetic Prandtl, and Lundquist numbers, respectively.[21]

In our simulations, we define the reconnection time as the time from when the X point is formed until the formation of the largest closed flux volume. The reconnection time

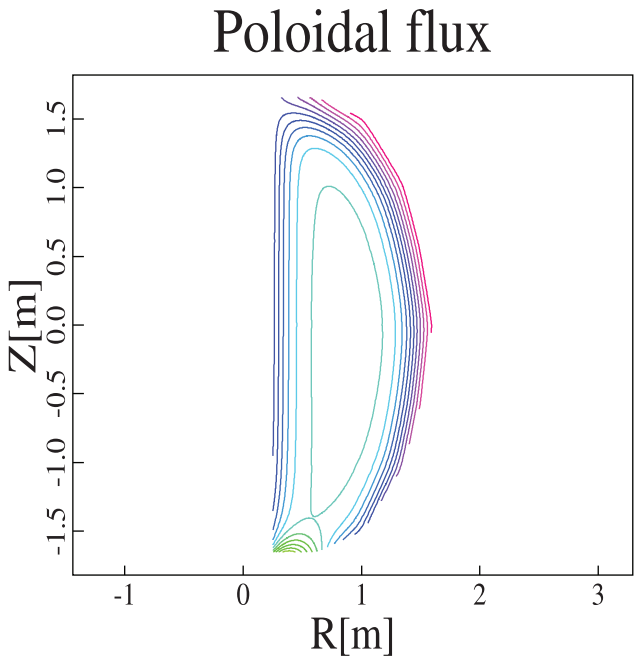

FIG. 5. Flux surfaces for for $\eta = 8\,m^2/s$ ($T_e \approx 14$ eV), $\Psi_{inj} \sim 22$ mWb at t = 9.55 ms.

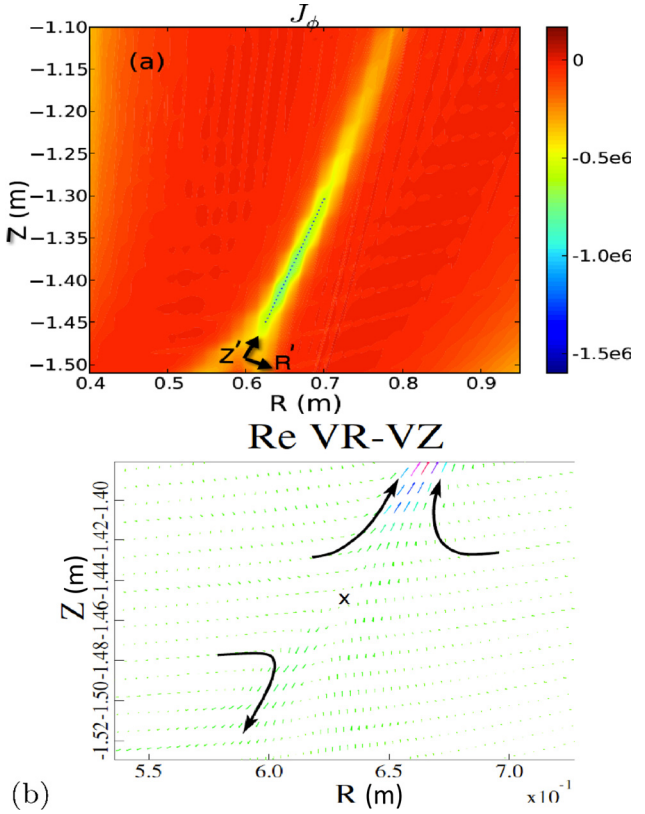

FIG. 6. (a) Elongated current sheet formed, for simulations with $T_e \approx 14$ eV. The arrows show the coordinate along current sheet (R', Z'). (b) Vector plot of poloidal flow during reconnection. X point forms at R = 0.63 m, Z = −1.445 m where the poloidal flow is zero. The arrows show the direction of inflow and outflows during reconnection.

observed in these NIMROD simulations for the temperatures 25, 14, and 5 eV are 0.49, 0.4, and 0.12 ms (at fixed $I_{inj} \approx 37$ kA). These numerical reconnection times are consistent with the theoretical Sweet-Parker reconnection time, $\tau_A\sqrt{S}(1+Pm)^{1/4}$, which are 0.5, 0.34, and 0.15 ms for the temperatures 25, 14, and 5 eV, respectively. We have used local reconnecting magnetic field of about 0.01 T for the Alfvén time (a/V_A, with a = 0.6 m and $n = 4\times10^{18}\,m^{-3}$) and the current sheet scale length ($L \sim 0.2$ m) for the resistive diffusion time (L^2/η). Thus, as expected from Sweet-Parker reconnection, the field lines both reconnect and diffuse faster as the temperature is reduced (or Lundquist number is reduced). Temperatures 14–25 eV are more relevant to experimental temperatures in transient CHI discharges in NSTX.

To better analyze the local reconnection process, in particular the plasma flow dynamics, we perform a coordinate transformation to coordinates aligned with the current sheet. Figure 6 shows an elongated current sheet and the vector plot poloidal flow during the X point formation of the simulations with $T_e \approx 14$ eV and $\Psi_{Inj} \approx 55$ mWb presented in Sec. IV. As expected, the poloidal flow is zero around the X point shown in Fig. 6(b). The Sweet-Parker type structure of inflow and outflow are clearly seen in the coordinate along the elongated current sheet (Fig. 6(b)). The structure of the inflow pinch (V_R') with respect to the coordinate perpendicular to the current sheet (R') is shown in Fig. 7. Consistent with the bidirectional pinch force, a radial pinch E × B flow is generated to bring the field lines together to reconnect as

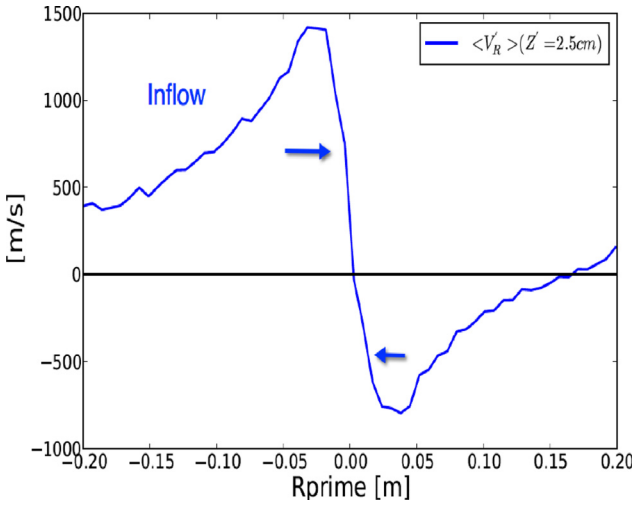

FIG. 7. Inflow pinch profile during reconnection.

explained above.[8] In the coordinate of the current sheet, the structure of outflow is also consistent with Sweet-Parker reconnection [Fig. 8(a)] and its peak value can approach the poloidal Alfvén velocities $[V_{out} \approx V_{A(\mathrm{pol})} = B_{in}/\sqrt{\mu_0 \rho}$, where the reconnecting field B_{in} is $B_z \approx 0.0118$ T], of about 90 km/s at zero viscosity. At fixed magnetic diffusivity, viscosity can modify the outflows according to the Sweet-Parker model as $V_{out}/V_A = 1/\sqrt{1+Pm}$. We have performed simulations at different Pm, where magnetic diffusivity is fixed but viscosity is varied. Figure 8(b) shows the resulting outflows $(V_{out}/V_{A(\mathrm{pol})})$ from the simulations for four values of Pm. As it is seen, the maximum outflows at Pm = 1 reaches 60 km/s. It is also found that the resulting outflows are consistent with values from the Sweet-Parker model, as shown in Fig. 8(b) by the solid line.

We finally verify the importance of terms in Ohm's law during the reconnection process in the injector region. The inductive term, $(\mathbf{V} \times \mathbf{B})$, and the dissipative term, ηJ, in Ohms law provide different contributions during the resistive reconnection. We first find that an electric field is induced in the toroidal direction (loop voltage). The induced electric field causes the evolution of the poloidal flux during the reconnection. At high values of magnetic diffusivity, when reconnection does not occur (shown in Fig. 3), the profiles of $(\mathbf{V} \times \mathbf{B})_\phi$ and ηJ_ϕ around the injector region are shown in Figs. 9(a) and 9(b). As seen around the injector region (R = 0.5–0.7 m), the induced electric field changes sign after the voltage is turned off while the current density in this region is almost zero (i.e., the poloidal flux has decayed in this region) [Fig. 9(b)]. For the low magnetic diffusivity case $(\eta = 8\,\mathrm{m}^2/\mathrm{s})$, we also note that the induced emf changes sign after the injector voltage is turned off, as seen from the $(\mathbf{V} \times \mathbf{B})_\phi$ profiles before and during reconnection in Figs. 9(c) and 9(d). The change of sign of induced toroidal electric field (loop voltage) is an indication of the poloidal flux evolution before and after reconnection, but is not sufficient to characterize the reconnection process. We then verify the toroidal component of the Ohm's law around the injection region during the X point formation. The profiles of the toroidal induced electric field (emf), $-(\mathbf{V} \times \mathbf{B})_\phi$ and ηJ_ϕ around the injector region, are shown in Fig. 9(d). As expected from the Sweet-Parker model, there is a clear separation between the outer ideal region and the inner reconnection layer, that is, the toroidal ideal emf $(\mathbf{V} \times \mathbf{B})$ is important outside the reconnection layer and the diffusive resistive term (ηJ_ϕ) is important inside the reconnection layer (≈0.63 m).

IV. INJECTOR FLUX

It has been shown that the ratio of the total current to the injector current scales with the ratio of the toroidal flux to the injector flux.[12,22] The scaling of some of the overall macroscopic behavior of the plasma during CHI, including the scaling of CHI-generated current with the toroidal and injector fluxes have been confirmed using 2-D TSC and NIMROD simulations.[13,23] Here, in order to investigate the effect of injector flux on the physics of flux closure in transient CHI, we perform simulations for four different values of injector flux (Ψ_{inj}) of about 55 mW, 44 mWb, 27 mWb, and 22 mWb (all with $V_{\mathrm{inj}} \sim 1$kV). The injector flux is changed via the divertor coil currents shown in Fig. 1.

Time histories of injector current and total plasma current are shown in Fig. 10. Consistent with earlier predictions, both the injector current and the total current are reduced when the injector flux is lowered. The reduction in the plasma current for the lower injector flux case is consistent with the requirement that in the absence of dynamo current drive, total plasma current scales with the magnitude of the

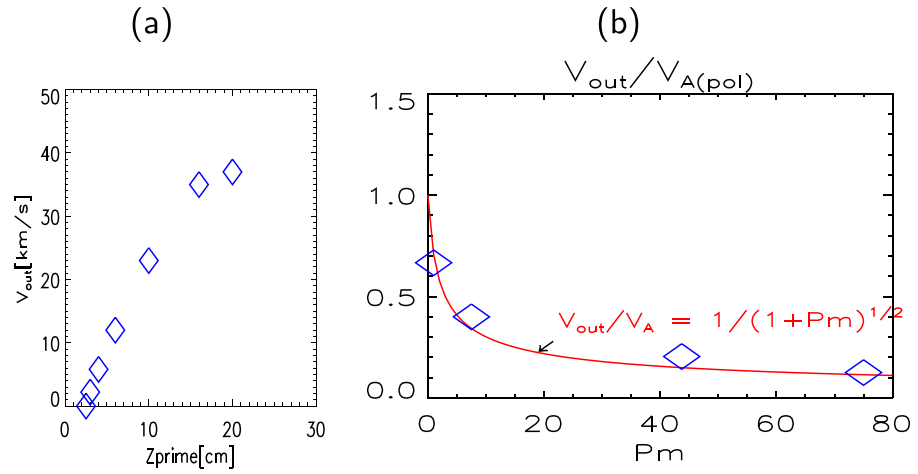

FIG. 8. (a) Maximum outflow vs. Z' along the current sheet (Pm = 7.5) (b) The ratio of maximum outflows to the poloidal Alfvén velocity $V_{out}/V_{A(\mathrm{pol})}$ vs. magnetic Prandtl number. The magnetic diffusivity is fixed $(\eta = 8\,\mathrm{m}^2/\mathrm{s})$ and viscosity is varied.

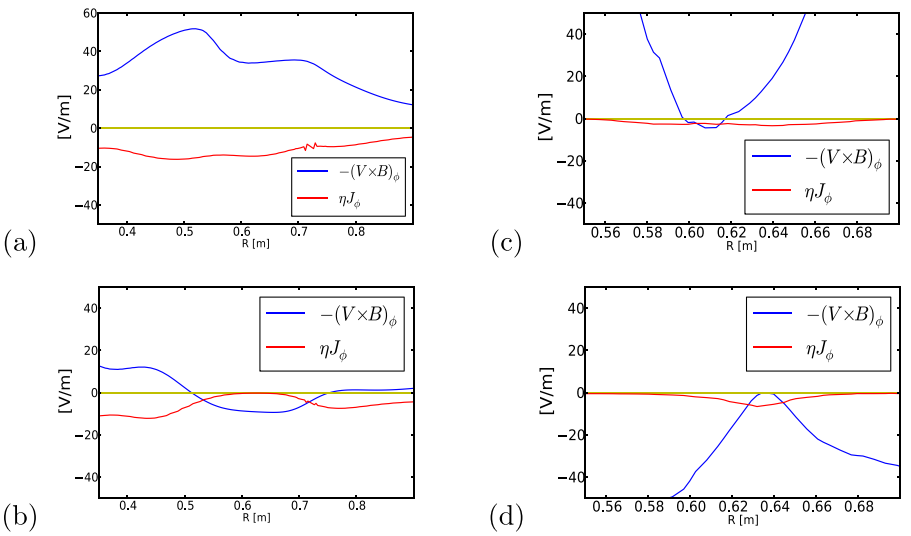

FIG. 9. Profiles of induced toroidal electric field $-(\mathbf{V}\times\mathbf{B})_\phi$ and ηJ_ϕ (at $z=-1.4\,m$) (a) and (b) for $\eta = 100\,m^2/s$ ($T_e \approx 2.7\,eV$) before and after the voltage are turned off, at $t=8.9\,ms$ and $t=9.05\,ms$, respectively; (c) and (d) for $\eta = 8\,m^2/s$ ($T_e \approx 14\,eV$), (c) before reconnection at $t=8.99\,ms$ (d) during the X point formation at $t=9.01\,ms$.

injector flux. This is because the injected open-field line poloidal flux that reconnects generates the closed flux configuration. The reduction in the injector current is much larger and approximately reflects a stronger dependence of the injector flux as noted in the 0-d model of Jarboe.[12,13,24] These simulations, which are at magnetic diffusivity of $\eta = 8\,m^2/s$ (equivalent to Te = 14eV), show formation of X point and closed flux surfaces. We find that the fraction of closed flux current appears to remain the same (about 11%) for all these four cases. These simulations therefore show that changing the injector flux via changing the helicity injection rate, directly change the resulting macroscopic plasma and injector currents, suggesting that to increase the *magnitude* of the closed flux, the *magnitude* of the injector flux should be increased. However, the microscopic reconnection process and the fraction of closed flux current to the total plasma current are not significantly affected by the magnitude of the injector flux. We also note that the rate of decrease of the injector current and total current mainly depends on the magnetic diffusivity.

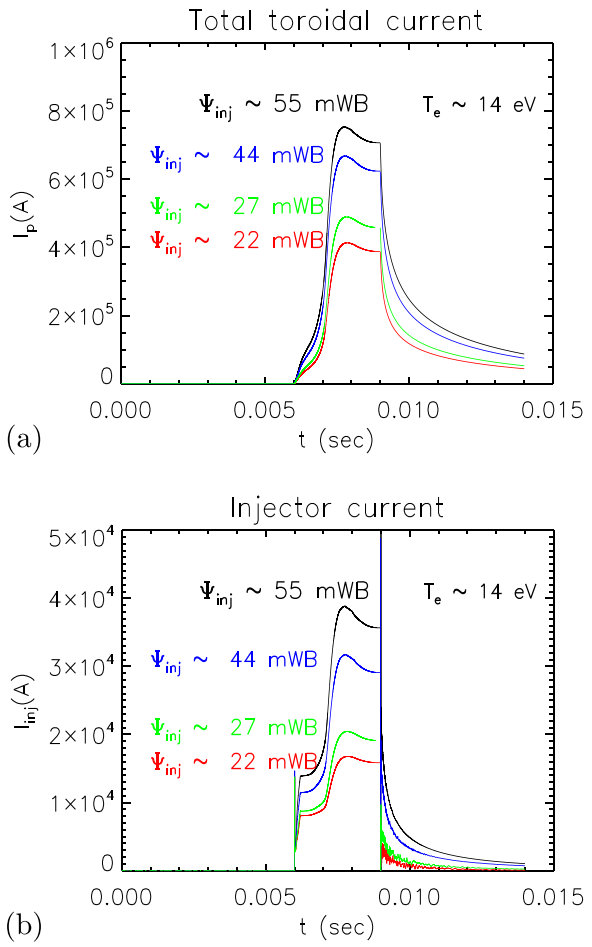

FIG. 10. Time histories of (a) the total toroidal current at different values of the injector flux of about 55 mW, 44 mWb, 27 mWb, and 22 mWb, and (b) the corresponding injector currents for the same values of the injector flux.

V. INJECTOR FLUX FOOTPRINT WIDTH

In addition to injector flux, another important effect that can alter the maximum closed flux formation is the width of the injector flux footprint on the divertor plates. This notion has also been described in Ref. 12. Through adjusting the direction and magnitude of lower divertor coil currents, this width can be changed. To examine this effect, we perform simulations with different injector flux footprint width for a current of −4600 A in the primary injector coil (PF1B coil as shown in Fig. 1). By reversing the direction of currents in the lower divertor coils (PF2L = −4000 A and PF1AL = −800 A), the width of injector footprint is increased as shown in Fig. 11(a). To obtain the narrower footprint shown in Fig. 11(b), we use PF2L = 500 A and PF1AL = 800 A. We find that the closed flux fraction increases as the injector flux footprint width is reduced. As seen from the Poincaré plots at the time of the maximum flux closure in Fig. 12, only a small volume of closed surfaces forms for the wide footprint case. The ratio of closed current to the total plasma current is only 1.8% for wide footprint, but this ratio is increased to 12% for the narrow footprint case. When the current in PF2L coils is further increased to 1000 A, we find a larger closed current ratio of about 13%–16%. The distance between the injector flux footprints is therefore important for driving an effective magnetic reconnection process and maximum flux closure, and imply that at a given value of the primary injector flux coil current

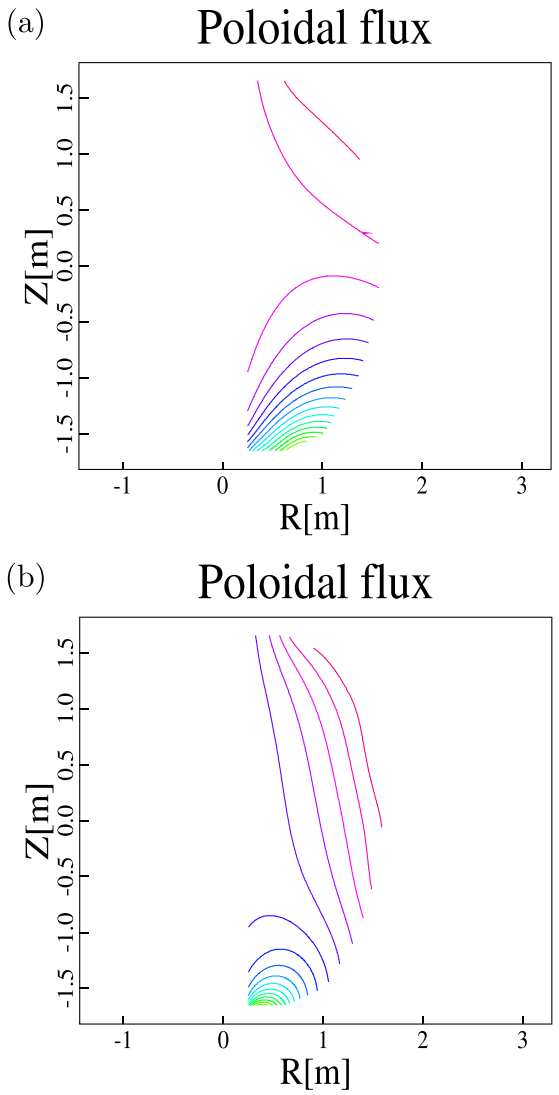

FIG. 11. Initial poloidal injector fluxes for (a) wide footprint (b) narrow footprint cases.

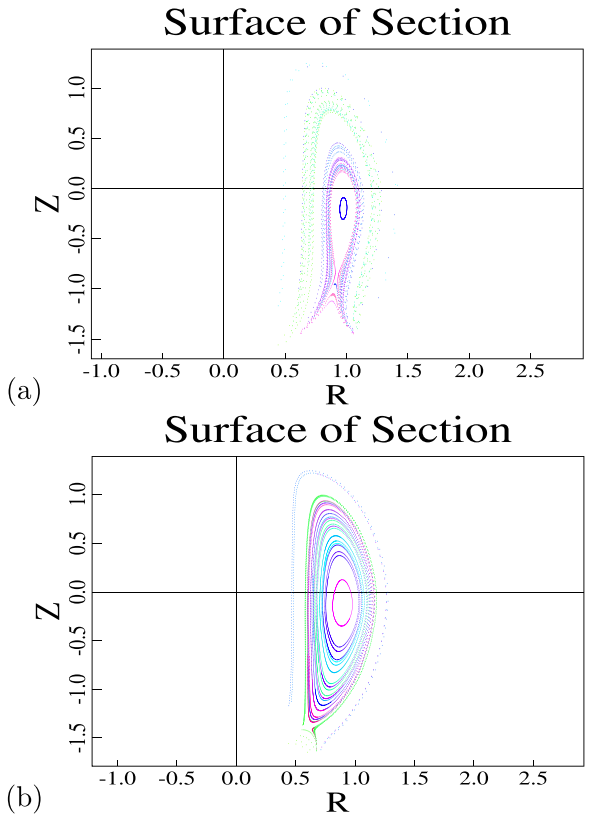

FIG. 12. Poincaré plots for the two cases with different footprint width shown in Fig. 11 for (a) wide footprint case at t = 9.75 ms ($I_{inj} \approx$ 29kA, $\Psi_{inj} \sim 74$ mWb) and (b) for narrow footprint case at t = 9.6 ms ($I_{inj} \approx$ 10kA, $\Psi_{inj} \sim 24$ mWb), $\eta = 8\,m^2/s$ ($T_e \approx 14$ eV).

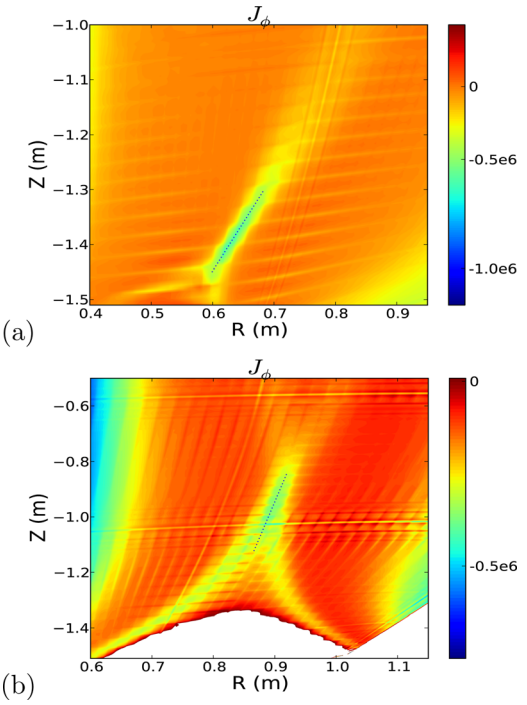

FIG. 13. Localized current sheets formations during reconnection (a) narrow (b) wide footprint cases.

(−4600 A current in PF1B), but with different coil currents for flux shaping, the magnitude of the closed flux can be increased by reducing the injector flux foot print width.

In these simulations, the current sheet and X point are formed at different locations. When the footprint is wide, the current sheet (and X point) is formed far from the injector gap, around R = 0.85 m (Fig. 13(b)). However, for the narrow footprint case with larger closed flux volume, the elongated current sheet forms close to the injector slot (Fig. 13(a)). The outflows in the narrow foot print simulation can reach up to 8500 m/s. However, we find that the outflows are not significant during the weak reconnection process in the wide footprint simulations.

In these simulations, which have the same magnetic diffusivity of $\eta = 8\,m^2/s$ (and similar resistive time scale), we can further investigate the reconnection time, and the contribution of Alfvénic time scales in the reconnection process. The reconnection time (τ_{rec}) defined here as the time from when the X point is formed until the formation of the largest closed flux volume is about 0.4 ms and 0.58 ms for the wide and narrow foot print cases, respectively. Thus, the reconnection times for these simulations (with the same η) exhibit clear dependency to the Alfvén time scales. The reconnecting magnetic fields in the current sheet coordinate

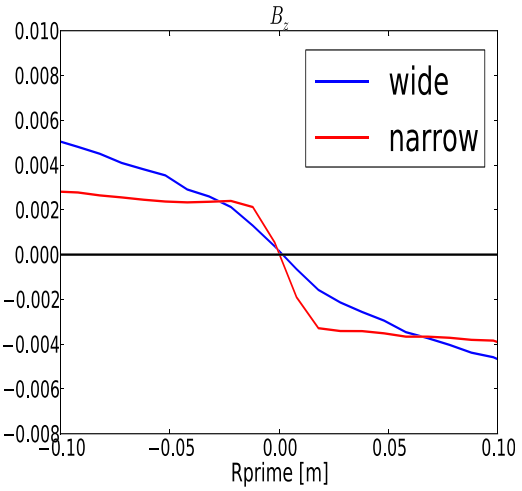

FIG. 14. The reconnecting magnetic field in the current sheet coordinates for the simulations with two injector footprints shown in Fig. 11.

at around the midpoint of the current sheet are plotted in Fig. 14 showing different magnitude. Thus, for the cases with different injector footprints, the Alfvén times calculated from the reconnecting fields (Fig. 14) may vary (the density is the same). Using the reconnecting magnetic fields at $R^{'} = 0.1$ and -0.1 shown in Fig. 14, the estimation of Alfvén times ($\tau_A = a/V_A$ with a = 0.6 m) for the wide footprint and narrow footprint cases is $1.65e^{-5}$ s and $2.4e^{-5}$ s, respectively. The theoretical Sweet-Parker reconnection time, $\tau_A\sqrt{S}(1+Pm)^{1/4}$, is then obtained as 0.49 ms and 0.59 ms for the wide and narrow footprint cases, respectively. These calculated S-P reconnection times are consistent with the numerical reconnection times obtained from the simulations. We should note that the reconnection time for a simulation with narrow footprint with increased PF2L currents of 1000 A and with much lower injector current is about 0.73 ms, which is longer than the two other cases. This is because at lower injector current, the reconnecting field is smaller around the current sheet resulting in longer Alfvén time.

VI. RATE OF INJECTOR VOLTAGE AND CURRENT REDUCTION

In all the simulations presented above, similar to the experiment, the injector voltage is turned off instantaneously at 9 ms. Here, we study the effect of the rate of injector voltage and injector current reduction on the flux closure, and find that it can significantly affect the maximum volume of flux closure. We perform three sets of simulations where the rate of reduction of voltage is varied. Figure 15(a) shows three sets of injector voltage used and resulting total plasma current for each simulation. For case 1, the voltage is ramped down slowly and at t = 15 ms is set to zero. The plasma current decays very slowly as the injector voltage is reduced, and X point and a small volume of flux closure only formed after 15 ms. For the second case, the voltage ramped down to zero at t = 12 ms. A slightly larger volume of closed flux surfaces formed after 12 ms as shown in Fig. 16(b). Case 3 is when the voltage is turned off instantaneously at t = 9 ms. Maximum closed flux current is about 40 kA, 8 kA, and 1 kA for cases 3–1, respectively. We therefore find that rapidly reducing the

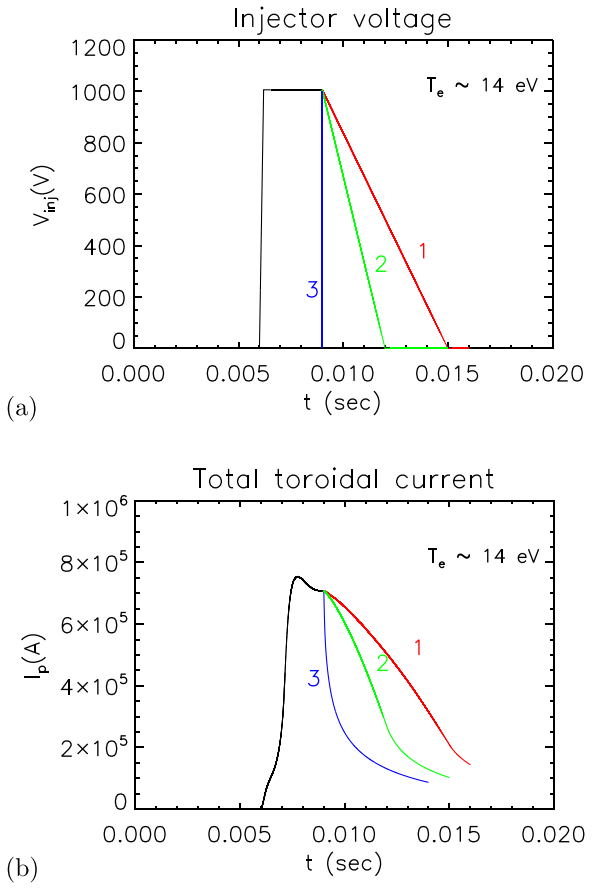

FIG. 15. Time histories of (a) injector voltage (b) total plasma current for three cases with different reduction rate of injector voltage.

injector voltage (and current) increases closed flux current. These results suggest that in transient CHI, at a given value of the injector flux and injector flux foot-print width, the magnitude of the generated close flux current can be increased by reducing the injector voltage (and thus the injector current) on as fast a time-scale as possible. This can be understood from the results from Secs. II, III and Ref. 8, which show that a more rapidly decreasing injector voltage (and injector current) increases the magnitude of the radial pinch flow (and the induced toroidal loop voltage), which is responsible for bringing the oppositely directed field lines together.

VII. SIMULATIONS WITH TEMPERATURE EVOLUTION

Here, we investigate the physics of flux closure using simulations at finite pressure. Simulations at zero pressure (constant temperature) presented above have elucidated the physics of magnetic reconnection during transient CHI. They have also provided better understanding of the critical requirements for flux surface closure. However, here we examine whether physics of heat transport may change the closed flux current. In this simulation, we also evolve plasma temperature and density. Anisotropic thermal conductivities, ohmic heating, and Spitzer resistivity ($\eta \propto T_e^{-3/2}$) are included in the pressure model

$$\frac{n}{(\Gamma-1)}\left(\frac{\partial T}{\partial t}+\mathbf{V}.\nabla T\right)=-p\nabla.\mathbf{V}-\nabla.\mathbf{q}+Q, \qquad (1)$$

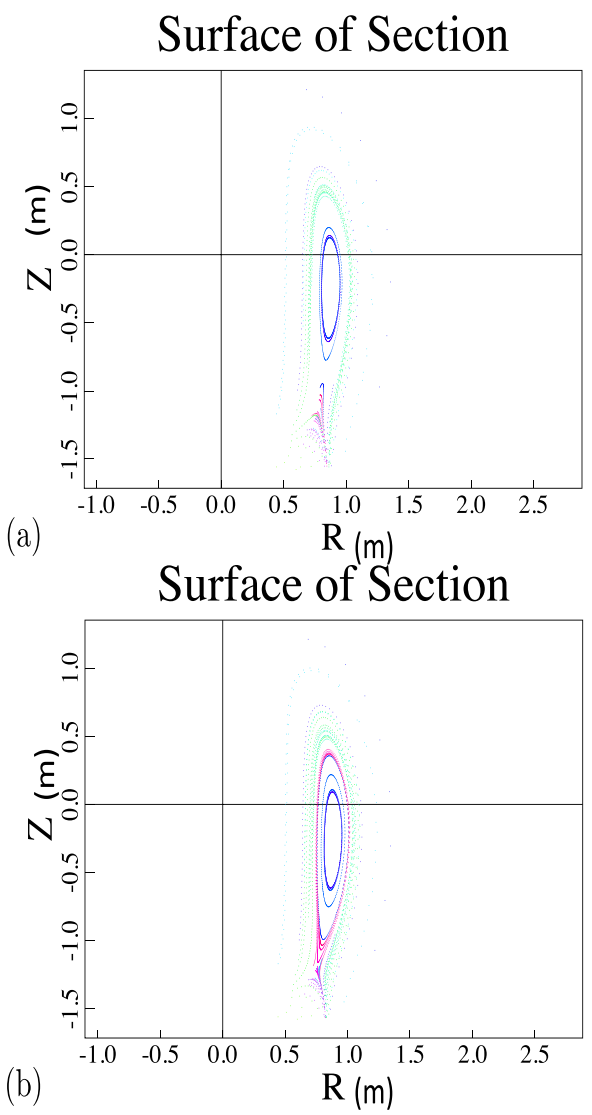

FIG. 16. Poincare plots for simulations with slow rampdown of injector voltage shown in Fig. 15 (a) case 1 at t = 15.7 ms (b) case 2 at t = 12.9 ms.

where $p = nkT$, $\mathbf{q} = -n[(\kappa_{||} - \kappa_{\perp})\hat{b}\hat{b} + \kappa_{\perp}\mathbf{I}] \cdot \nabla T$, $Q = \eta J^2$. A temperature-dependent thermal diffusivity along the magnetic field ($\kappa_{||} \propto T_e^{5/2}$) and a constant perpendicular thermal diffusivity ($\kappa_{\perp} = 2.5\,\mathrm{m}^2/\mathrm{s}$) are used. Simulations with the evolution of pressure due to ohmic heating and thermal transport have also been studied in Ref. 19. The model includes the time-dependent boundary conditions due to the evolution of the bias poloidal flux, radiation cooling, and other physics needed for detailed comparison with experiment. The injection voltage and current are driven by a model of the experimental power supply. Flux closure is found in the axisymmetric approximation and shown to be triggered by the magnetic pressure imbalance that forms when the voltage across the injection slot drops, resulting in a reduction of the plasma inflow from the slot. The closure characteristics are consistent with the Sweet-Parker process presented in this manuscript. The full-machine model is being extended to include density evolution associated with the inflow of injected plasma and other physics.

The finite pressure simulations presented here are with fixed boundary fields (fixed poloidal coil currents with $\Psi_{inj} \sim 55$ mWb), enabling a comparison of these results with the zero pressure simulation results presented above. In this simulation, total toroidal plasma current reaches a value of about 0.28MA. As in the zero pressure simulations, constant injector voltage (≈1.7 kV) is rapidly reduced at 9 ms. The X point starts to form after the fast drop of the voltage around 9.08 ms and the formation of fairly large volume of closed flux surfaces is shown in Fig. 17. The ratio of closed flux current to the total plasma current is about 14%–15%. This ratio is close to the value for the high temperature simulation with $T_e \sim 24$ eV shown in Fig. 3.

To further understand the cause of magnetic reconnection, we have isolated different physics terms (by excluding anisotropic heat conductivities, ohmic heating, and temperature-dependent resistivity) in different sets of simulations with temperature evolution. We find that starting with a 1 eV plasma, only when temperature dependent resistivity is present in the simulations, reconnection occurs. As plasma is heated by ohmic heating, due to temperate-dependent resistivity, at hot (and less resistive) plasma locations, current can easily flow and causes the flux to close on fast, experimental, time scales. Temperature profiles around the reconnection site (z = −1.3 m), before and after X point formation, are shown in Fig. 18(a), and in the core region shown in Fig. 18(b). The temperature in the region between R = 0.55–0.7 m is equilibrated after the X point formation and temperature reaches about 20 eV at the X point ($R \approx 0.67, Z = -1.3$). This is consistent with the current sheet formation at the reconnection site. In this region, due to the temperature-dependent resistivity local currents can flow easier to form a current sheet around R = 0.67 m. The equilibration of temperature further continues in the closed flux surface region as the closure occurs. The plasma core in the closed flux region is heated to about 28 eV at the midplane as shown in Fig. 18(b) from the profile at t = 9.87 ms. The temperature in the plasma core region (in the closed flux region) does not exceed 30 eV. In the regions of open flux surfaces (R = 0.4 m), there are layers of hot plasma with temperature up to 100 eV, which is higher than the experimental

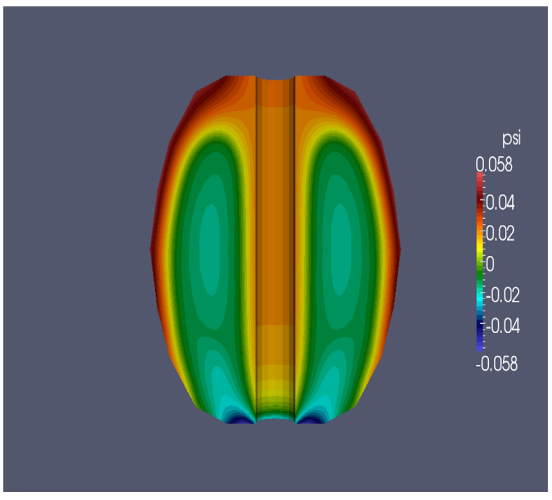

FIG. 17. Poloidal flux surfaces from simulation with temperature evolution, during the flux closure at t = 9.87 ms ($\Psi_{inj} \sim 55$ mWb, $V_{inj} \approx 1.7$ kV).

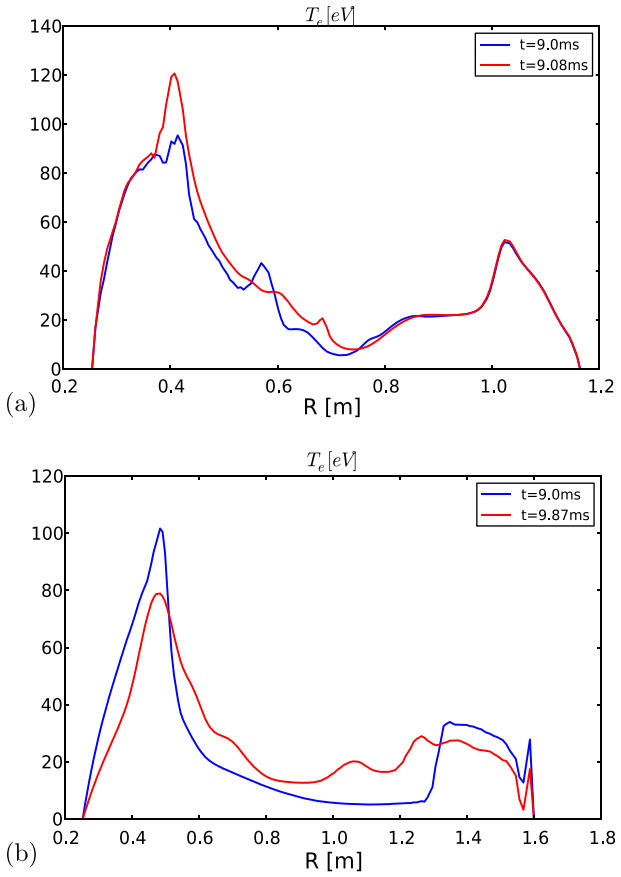

FIG. 18. Temperature profiles at (a) z = −1.3 around X point at 9 ms and right after X point formation (b) z = 0 at midplane at 9 ms and during flux closure at t = 9.87 ms.

values. More comprehensive transport modeling (including radiation cooling modeling) is currently being investigated for further validation with the experimental values and will be reported in the future.

VIII. SUMMARY

Using resistive MHD simulations, we have investigated transient CHI in NSTX. These MHD simulations show that in the right parameter regimes, a local 2-D Sweet-Parker type reconnection is triggered in the injector region and closed flux surfaces are formed in the global domain. Nonaxisymmetric 3-D disturbances appear not to be important in the formation of closed flux surfaces.[19] However, for a complete picture of the reconnection process, both local and global length scales, as well as both ideal Alfvénic and resistive time scales are resolved in these simulations.

In this paper, we examine four primary effects for flux closure, 1—magnetic diffusivity, 2—injector flux, 3—injector flux footprint, 4—the rate of injector voltage and current reduction. We first find that magnetic diffusivity (temperature) should be low (high) enough to allow an effective reconnection with large volume of closed flux surfaces. Local Sweet-Parker signatures are also verified in our simulations. These signatures include formation of an elongated current sheet $(L \gg \delta)$, inflow pinch flows and outflows along the elongated current sheet are demonstrated. It is found that the outflows in our visco-resistive simulations scale with magnetic Prandtl number and can approach the poloidal Alfvénic flows at low magnetic Prandtl numbers.

Second, we find that both total plasma current and injector current scale with injector flux, consistent with earlier predictions. However, the microscopic reconnection process and the fraction of closed flux current are not significantly affected by the magnitude of the injector flux. Third, simulations with different injector flux footprint width have shown a significant effect on the fraction of closed current and as the injector flux footprint becomes narrower, the ratio of closed flux current increases. Fourth, we find that the rate of injector voltage reduction also strongly affects the maximum volume of closed surfaces and closed flux current. The most rapid reduction of injector voltage shows the largest closed flux current. Finally, by including a temperature evolution model, we find a closed flux current ratio similar to the zero pressure simulations at low magnetic diffusivity $(T_e \sim 25\,\text{eV})$. The present work is in the framework of resistive MHD. Possible importance of Hall effect on the reconnection process and flux closure will be studied in a future work.

ACKNOWLEDGMENTS

This work was supported by DOE-FG02-12ER55115 and the NSF frontier Center for Magnetic Self-Organization (CMSO). F.E. thanks S. Kaye for his valuable comments for the invited talk. We also thank A. Boozer for enlightening discussions.

[1]J. E. Menard, M. G. Bell, R. E. Bell, S. Bernabei, J. Bialek, T. Biewer, W. Blanchard, J. Boedo, C. E. Bush, M. D. Carter *et al.*, Nucl. Fusion **47**, S645 (2007).
[2]D. A. Gates, J. Ahn, J. Allain, R. Andre, R. Bastasz, M. Bell, R. Bell, E. Belova, J. Berkery, R. Betti *et al.*, Nucl. Fusion **49**, 104016 (2009).
[3]Y.-K. M. Peng, P. J. Fogarty, T. W. Burgess, D. J. Strickler, B. E. Nelson, J. Tsai, C. A. Neumeyer, R. Bell, C. Kessel, J. Menard *et al.*, Plasma Phys. Controlled Fusion **47**, B263 (2005).
[4]R. Raman, D. Mueller, B. A. Nelson, T. R. Jarboe, S. Gerhardt, H. W. Kugel, B. Leblanc, R. Maingi, J. Menard, M. Ono *et al.*, Phys. Rev. Lett. **104**, 095003 (2010).
[5]K. Hanada, H. Zushi, H. Idei, K. Nakamura, M. Ishiguro, S. Tashima, E. I. Kalinnikova, M. Sakamoto, M. Hasegawa, A. Fujisawa *et al.*, Plasma Sci. Technol. **13**, 307 (2011).
[6]M. Uchida, T. Yoshinaga, H. Tanaka, and T. Maekawa, Phys. Rev. Lett. **104**, 065001 (2010).
[7]A. Ejiri, Y. Takase, H. Kasahara, T. Yamada, K. Hanada, K. N. Sato, H. Zushi, K. Nakamura, M. Sakamoto, H. Idei *et al.*, Nucl. Fusion **46**, 709 (2006).
[8]F. Ebrahimi, E. B. Hooper, C. R. Sovinec, and R. Raman, Phys. Plasmas **20**, 090702 (2013).
[9]E. N. Parker, J. Geophys. Res. **62**, 509, doi:10.1029/JZ062i004p00509 (1957).
[10]P. A. Sweet, in *Electromagnetic Phenomena in Cosmical Physics*, edited by B. Lehnert (1958), Vol. 6 of IAU Symposium, p. 123.
[11]T. H. Jensen and M. S. Chu, Phys. Fluids **27**, 2881 (1984).
[12]T. R. Jarboe, Fusion Technol. **15**, 7 (1989).
[13]R. A. Bayliss, C. R. Sovinec, and A. J. Redd, Phys. Plasmas **18**, 094502 (2011).
[14]R. Raman, T. R. Jarboe, B. A. Nelson, V. A. Izzo, R. G. O'Neill, A. J. Redd, and R. J. Smith, Phys. Rev. Lett. **90**, 075005 (2003).

[15]R. Raman, B. A. Nelson, M. G. Bell, T. R. Jarboe, D. Mueller, T. Bigelow, B. Leblanc, R. Maqueda, J. Menard, M. Ono *et al.*, Phys. Rev. Lett. **97**, 175002 (2006).
[16]M. Nagata, T. Kanki, N. Fukumoto, and T. Uyama, Phys. Plasmas **10**, 2932 (2003).
[17]B. S. Victor, T. R. Jarboe, A. C. Hossack, D. A. Ennis, B. A. Nelson, R. J. Smith, C. Akcay, C. J. Hansen, G. J. Marklin, N. K. Hicks *et al.*, Phys. Rev. Lett. **107**, 165005 (2011).
[18]T. Kanki, M. Nagata, and Y. Kagei, Plasma Fusion Res. **5**, S2055 (2010).
[19]E. B. Hooper, C. R. Sovinec, R. Raman, F. Ebrahimi, and J. E. Menard, Phys. Plasmas **20**, 092510 (2013).
[20]C. R. Sovinec, A. H. Glasser, T. A. Gianakon, D. C. Barnes, R. A. Nebel, S. E. Kruger, D. D. Schnack, S. J. Plimpton, A. Tarditi, M. Chu *et al.*, J. Comput. Phys. **195**, 355 (2004).
[21]D. Biskamp, *Magnetic Reconnection in Plasmas* (Cambridge University Press, Cambridge, 2000).
[22]J. E. Menard, S. Gerhardt, M. Bell, J. Bialek, A. Brooks, J. Canik, J. Chrzanowski, M. Denault, L. Dudek, D. A. Gates *et al.*, Nucl. Fusion **52**, 083015 (2012).
[23]R. Raman, S. C. Jardin, J. Menard, T. R. Jarboe, M. Bell, D. Mueller, B. A. Nelson, and M. Ono, Nucl. Fusion **51**, 113018 (2011).
[24]A. J. Redd, T. R. Jarboe, B. A. Nelson, R. G. O'Neill, and R. J. Smith, Phys. Plasmas **14**, 112511 (2007).